Research Square

Preprints are preliminary reports that have not undergone peer review.
They should not be considered conclusive, used to inform clinical practice,
or referenced by the media as validated information.

Graphene-interlayer-induced suppression of the longitudinal spin Seebeck effect in Pt/Y 3 Fe 5 O 12 heterostructures

Jung-Min Cho
Chung-Ang University
Yun-Ho Kim
Chung-Ang University
Jae Won Choi
Chung-Ang University
Seong-Joon Won
Chung-Ang University
Gil-Sung Kim
Chung-Ang University
Young-Gui Yoon
Chung-Ang University
Sang-Kwon Lee
sangkwonlee@cau.ac.kr

Chung-Ang University

Research Article

Keywords: Proximity-induced magnetization · Longitudinal spin Seebeck effect · Ferromagnetic insulator · Monolayer graphene · Spin mixing conductance · First-principles calculation

Posted Date: November 13th, 2026

DOI: https://doi.org/10.21203/rs.3.rs-11470694/v1

License: This work is licensed under a Creative Commons Attribution 4.0 International License.
Read Full License

Additional Declarations: No competing interests reported.

Graphene-interlayer-induced suppression of the longitudinal spin Seebeck effect in $Pt/Y_3Fe_5O_{12}$ heterostructures

Jung-Min Cho†, Yun-Ho Kim†, Jae Won Choi, Seong-Joon Won, Gil-Sung Kim, Young-Gui Yoon*, and Sang-Kwon Lee*

[1] Department of Physics, Chung-Ang University, Seoul 06974, Republic of Korea

†These authors contributed equally to this work.

*Address correspondence to yyoon@cau.ac.kr and sangkwonlee@cau.ac.kr

Abstract

We investigate the influence of sequentially inserted graphene (Gr) interlayers on thermally driven spin transport in Pt/YIG, Pt/Gr/YIG, and Pt/Gr/Gr/YIG heterostructures through magnetic-field- and temperature-dependent longitudinal spin Seebeck effect (LSSE) measurements. The LSSE voltage exhibits a characteristic magnetic-field-dependent polarity reversal and increases approximately linearly with the applied temperature difference. Compared with Pt/YIG, the LSSE signal decreases to approximately 47% of the reference value upon insertion of a single Gr layer and is further reduced to approximately 22% of the original response with two Gr layers, demonstrating successive suppression of the measured LSSE response. The Pt/Gr/Gr/YIG heterostructure exhibits a nonmonotonic temperature dependence, with a maximum LSSE response near 150 K. To investigate the underlying interfacial electronic structure, density functional theory (DFT) calculations were performed for Pt/Gr/Gr/NiFe model heterostructures with AA- and AB-stacked bilayer Gr, using NiFe as a simplified ferromagnetic model. The calculated electronic structures reveal stacking-dependent changes in electronic states near the Fermi level, providing a possible microscopic framework for understanding Gr-mediated modifications of interfacial spin transmission. These findings highlight Gr layer number and stacking configuration as potential parameters for controlling interfacial spin transport in magnetic heterostructures.

Keywords Proximity-induced magnetization · Longitudinal spin Seebeck effect · Ferromagnetic insulator · Monolayer graphene · Spin mixing conductance · First-principles calculation

1. Introduction

The spin Seebeck effect (SSE) has attracted considerable attention in spin caloritronics because it enables the generation of spin currents driven by a temperature gradient without the direct flow of charge carriers [1-3]. When a magnetic material is subjected to a temperature gradient, thermally excited magnons can transfer spin angular momentum across the interface into an adjacent nonmagnetic metal (NM). The injected spin current is subsequently converted into a transverse electric voltage through the inverse spin Hall effect (ISHE), arising from spin–orbit coupling in the NM [4]. In particular, the longitudinal spin Seebeck effect (LSSE), in which the thermally generated spin current propagates parallel to the applied temperature gradient, provides a useful platform for investigating spin transport in magnetic-insulator/metal heterostructures (Fig. 1a). Among various magnetic materials, yttrium iron garnet ($Y_3Fe_5O_{12}$, YIG) has been extensively studied because of its exceptionally low magnetic damping, electrically insulating nature, and efficient magnon transport properties. Consequently, Pt/YIG heterostructures have become representative systems for studying thermally driven spin injection and spin-to-charge conversion [5]. The magnitude of the LSSE is determined not only by the generation and propagation of thermally excited magnons in YIG but also by the efficiency of spin angular momentum transfer across the YIG/Pt interface (Figs. 1b–c). Within the thermal spin pumping framework, the interfacial spin current density can be approximately expressed as [6]

$$\boldsymbol{J}_{\mathrm{s}} = \frac{\hbar\, g_{\mathrm{eff}}^{\uparrow\downarrow}\, \gamma\, k_{\mathrm{B}}}{2\pi\, M_{\mathrm{s}}\, V_{\mathrm{a}}} (T_{\mathrm{m}} - T_{\mathrm{e}}), \tag{1}$$

where $\boldsymbol{J}_{\mathrm{s}}$ is the interfacial spin angular momentum current density, $g_{\mathrm{eff}}^{\uparrow\downarrow}$ is the real part of the interfacial spin mixing conductance per unit area, γ is the gyromagnetic ratio, k_{B} is the Boltzmann constant, l_{th} is the characteristic thermal length, M_{s} is the saturation magnetization of YIG, and V_{a} is the temperature-dependent magnetic coherence volume. Here, T_{m} and T_{e} represent the magnon

temperature in YIG and the electron temperature in Pt at the interface, respectively. This simplified expression describes the thermal spin pumping contribution driven by the magnon-electron temperature difference. It indicates that the interfacial spin current is closely related to the effective spin mixing conductance, which characterizes the efficiency of spin angular momentum transfer across the interface. The injected spin current is subsequently converted into a transverse charge current through the ISHE in Pt, expressed as [4, 7]

$$\boldsymbol{J}_c^{\mathrm{ISHE}} = \theta_{\mathrm{SH}} \frac{2e}{\hbar} \boldsymbol{J}_{\mathrm{s}} \times \boldsymbol{\sigma}, \tag{2}$$

where θ_{SH} is the spin Hall angle of Pt, e is the elementary charge, and $\boldsymbol{\sigma}$ is the unit vector along the spin polarization direction. Here, $\boldsymbol{J}_{\mathrm{s}}$ represents the spin angular momentum current density directed along the spin-flow direciton. These relations suggest that the LSSE voltage is sensitive to both the thermal magnon excitation in YIG and the interfacial spin transmission efficiency. Therefore, modification of the YIG/Pt interface provides an effective approach for controlling thermally driven spin transport. Previous studies have demonstrated that the LSSE response in Pt/YIG heterostructures is strongly influenced by the magnetic properties and interfacial conditions of YIG. In particular, magnetic anisotropy near the YIG surface can modify the magnetic-field dependence of the LSSE, leading to deviations between the LSSE response and the bulk magnetization behavior [5, 8]. Furthermore, Guo *et al.* systematically investigated the temperature-dependent LSSE in Pt/YIG heterostructures and demonstrated that the low-temperature enhancement of the LSSE depends strongly on the YIG thickness and interfacial conditions [9]. Their results indicated that the temperature dependence of the LSSE cannot be explained solely by bulk magnon transport but requires consideration of the spin transmission efficiency at the magnetic-insulator/metal interface. These observations highlight the importance of interfacial spin coupling in determining both the magnitude and temperature dependence of the LSSE.

Graphene (Gr), a two-dimensional material with high carrier mobility, weak intrinsic spin–orbit coupling (SOC), and potentially long spin relaxation lengths, has emerged as a promising material for controlling spin transport in magnetic heterostructures [10, 11]. When Gr is placed in contact with YIG, magnetic proximity effects can modify its electronic structure through interfacial exchange interactions, resulting in spin-dependent electronic states and magnetic responses [11, 12]. Such characteristics suggest that the insertion of Gr between Pt and YIG can significantly influence the interfacial spin transmission pathway. Indeed, previous spin-pumping measurements on Pt/Gr/YIG heterostructures demonstrated that the insertion of Gr reduces the effective spin mixing conductance and ISHE voltage, suggesting enhanced interfacial spin loss and reduced spin injection efficiency [13]. In addition, our previous study revealed that single- and multilayer Gr interlayers modify the surface magnetic anisotropy of YIG, as evidenced by changes in the magnetic-field dependence of the LSSE in Pt/YIG heterostructures [5]. These findings demonstrate that Gr acts not merely as a passive spacer but as an interfacial modifier capable of altering magnetic coupling and spin transport properties. Furthermore, previously reported first-principles calculations of Pt/Gr/NiFe heterostructures revealed Gr–metal hybridization and proximity-modified electronic states near the Fermi level, suggesting that Gr insertion can substantially reconstruct the interfacial electronic environment [14].

Despite these advances, the relationship between the number of Gr interlayers, temperature-dependent LSSE behavior, and microscopic interfacial electronic structure requires further investigation. In particular, although Gr-induced modifications of surface magnetic anisotropy and spin-pumping efficiency have been reported, the progressive suppression of thermally driven spin transmission by sequentially transferred monolayer (ML) Gr interlayers remains insufficiently understood. According to the thermal spin pumping framework, a reduction in the effective spin mixing conductance is expected to decrease the spin current injected into Pt, provided that the thermal

driving conditions and spin detection efficiency remain comparable. Moreover, temperature-dependent LSSE measurements can help distinguish changes in the overall spin transmission efficiency from modifications of the temperature-dependent magnon transport response. Combining these measurements with first-principles calculations may provide further insight into the electronic and magnetic origins of the interfacial spin attenuation. In particular, the electronic reconstruction associated with an additional Gr/Gr interface and different bilayer stacking configurations may provide a possible microscopic basis for understanding Gr-layer-dependent spin transmission.

In this study, we investigate the magnetic-field- and temperature-dependent LSSE in Pt/YIG, Pt/Gr/YIG, and Pt/Gr/Gr/YIG heterostructures with sequentially transferred ML Gr interlayers. The LSSE signal decreases to approximately 47% and 22% of the Pt/YIG reference value upon insertion of one- and two-ML Gr layers, respectively. The Pt/Gr/Gr/YIG heterostructure also exhibits a nonmonotonic temperature dependence, with a maximum LSSE response near 150 K. First-principles density functional theory (DFT) calculations of AA- and AB-stacked Pt/Gr/Gr/NiFe model heterostructures, using NiFe as a simplified ferromagnetic model, reveal stacking-dependent changes in the electronic structure near the Fermi level. These results suggest that Gr layer number and interfacial electronic coupling may contribute to the modulation of thermally driven spin transport.

2. Experimental Details

2.1. Sample preparation

To investigate the influence of ML Gr interlayers on thermally driven spin transport, three types of heterostructures, Pt/YIG, Pt/Gr/YIG, and Pt/Gr/Gr/YIG, were fabricated. Single-crystalline YIG films with a thickness of 2 μm were grown on gadolinium gallium garnet (GGG) substrates using liquid-phase epitaxy (LPE). Details of the growth process can be found in our previous studies [15]. Monolayer Gr was synthesized on Cu foils by low-pressure chemical vapor deposition (CVD),

following the procedure described in our previous study [5, 16]. The synthesized ML Gr was transferred onto YIG/GGG substrates using a poly(methyl methacrylate) (PMMA)-assisted wet-transfer method. After coating the Gr/Cu surface with PMMA, the underlying Cu foil was chemically etched, and the PMMA-supported Gr was rinsed with deionized water before being transferred onto the YIG surface. The PMMA support layer was subsequently removed using acetone [16]. For the Pt/Gr/YIG heterostructure, one ML Gr sheet was transferred onto the YIG surface, whereas the Pt/Gr/Gr/YIG heterostructure was fabricated by sequentially transferring two ML Gr sheets using the same wet-transfer procedure. The Pt/YIG heterostructure without a Gr interlayer was prepared as a reference sample. Finally, a 5-nm-thick Pt layer was deposited onto each sample by RF magnetron sputtering. The structural characteristics of the CVD-grown ML Gr were previously investigated using optical microscopy and micro-Raman spectroscopy [16].

2.2. Longitudinal spin Seebeck effect measurements in Pt/YIG

The LSSE was measured using a physical property measurement system (PPMS, DynaCool, Quantum Design, USA) over the temperature range of 25–300 K. The measurements were performed using a temperature-gradient configuration similar to that employed in our previous study [17]. Each sample was placed between two aluminum nitride (AlN) plates to establish a temperature difference along the out-of-plane direction. A micro-Peltier module was employed to generate and control the temperature difference across the sample assembly, while an oxygen-free copper block served as a thermal reservoir (Fig. 1a). For LSSE voltage measurements (V_{LSSE}), a temperature gradient (∇T) was applied along the out-of-plane direction, while a magnetic field was applied in-plane. The temperature difference (ΔT) was generated using a 100 Ω heater and monitored by an E-type thermocouple (Fig. 1a). ΔT was varied from 2 to 10 K, and the magnetic field was swept between −0.3 T and 0.3 T at 300 K. The resulting spin current was converted into a transverse voltage via the ISHE in Pt as shown

in Figs. 1b and 1c. Temperature-dependent measurements of V_{LSSE} were performed from 300 K to 25 K, with ΔT controlled at each temperature and the voltage recorded using a nanovoltmeter. The LSSE voltage coefficients ($V_{\mathrm{LSSE}}/\Delta T$)were compared among the Pt/YIG, Pt/Gr/YIG, and Pt/Gr/Gr/YIG heterostructures to evaluate the influence of the number of Gr interlayers on thermally driven spin transport.

2.3. First-principles DFT calculations

First-principles DFT calculations were performed using the Vienna Ab initio Simulation Package (VASP), following the computational framework described in our previous study [14]. In the present work, the calculations were extended to Pt/Gr/Gr/NiFe heterostructures containing two ML Gr layers with AA and AB stacking configurations. NiFe was employed as a simplified ferromagnetic model to investigate the influence of magnetic exchange coupling on the interfacial electronic structure. Both stacking configurations were structurally relaxed, and their electronic band structures were calculated with SOC included. The resulting electronic structures were analyzed to examine the influence of Gr interlayer coupling and stacking arrangement on the electronic states near the Fermi level, providing a qualitative perspective on Gr-mediated interfacial interactions relevant to the experimentally investigated Pt/Gr/Gr/YIG heterostructures.

3. Results and Discussion

3.1. Material characteristics

Figure 1d shows the high-resolution transmission electron microscopy (HR-TEM) image of the as-grown ML Gr transferred onto a TEM grid, revealing a locally well-ordered Gr lattice. The inset shows a well-defined sixfold symmetric fast Fourier transform (FFT) pattern characteristic of the two-dimensional honeycomb lattice of Gr, consistent with a lattice constant of approximately 2.46 Å [18-21]. Figure 1e shows the Raman spectra of CVD-grown ML Gr on a Cu substrate and ML Gr

transferred onto a YIG/GGG substrate. The as-grown ML Gr exhibits characteristic G and 2D bands at ~1588 and ~2698 cm^{-1}, respectively, corresponding to the first-order G mode and the second-order 2D mode [22-26]. The absence of a discernible D band suggests a relatively low defect density in the as-grown ML Gr [26]. After transfer onto YIG/GGG, the G and 2D bands are observed at ~1597 and ~2690 cm^{-1}, respectively. These spectral shifts may reflect changes in strain, charge doping, and interactions with the underlying substrate, although their individual contributions cannot be distinguished from the present Raman measurements alone [27]. These results support the successful synthesis and transfer of ML Gr onto the YIG/GGG substrate, with its characteristic Raman features retained after transfer.

3.2. LSSE measurements in Pt/YIG, Pt/Gr/YIG, and Pt/Gr/Gr/YIG heterostructures

Figure 2 shows that V_{LSSE} decreases successively from Pt/YIG to Pt/Gr/YIG and Pt/Gr/Gr/YIG at 300 K. All samples exhibit magnetic-field-dependent voltage polarity reversal and an approximately linear increase in V_{LSSE} with ΔT over the range of 2–10 K (Figs. 2a–d). At an applied magnetic field of 3 kOe, the LSSE coefficients are ~6.0, ~2.8, and ~1.3 $\mu V \cdot K^{-1}$, corresponding to approximately 60, 28, and 13 μV at ΔT = 10 K, respectively. Relative to Pt/YIG, V_{LSSE} is reduced to approximately 47% upon insertion of the first Gr layer and further to approximately 22% with the second Gr layer. Notably, Pt/Gr/Gr/YIG retains only approximately 46% of the Pt/Gr/YIG response, demonstrating pronounced stepwise suppression (Fig. 2e, f). Within the thermal spin-pumping framework, this attenuation is consistent with reduced effective spin-current transmission toward Pt, in line with previous spin-pumping and LSSE studies of Gr-containing heterostructures [13, 28]. In our heterostructures, Gr-induced modifications of interfacial magnetic coupling and YIG surface anisotropy may also influence the magnetic-field-dependent spin transmission, contributing to the observed LSSE suppression [5]. The second sequentially transferred Gr monolayer introduces an

additional Gr/Gr interface while preserving direct contact between Gr and YIG. Because the YIG spin source and Pt detection layer are retained, the additional attenuation highlights the sensitivity of the measured LSSE response to the intervening Gr-layer configuration. Nevertheless, changes in the measured LSSE voltage may also reflect differences in thermal coupling and spin-to-charge conversion conditions, and the present measurements do not independently determine the effective spin-mixing conductance**.** The pronounced attenuation therefore provides experimental evidence of layer-number-dependent modulation of the overall LSSE response, rather than a direct quantitative measurement of interfacial spin transparency. These findings establish sequential Gr insertion as an effective interface-engineering approach for stepwise control of the LSSE response.

3.3. Temperature-dependent LSSE measurements in Pt/Gr/Gr/YIG heterostructures

Figure 3 presents the magnetic-field- and temperature-dependent V_{LSSE} responses of Pt/Gr/Gr/YIG measured from 25 to 300 K at $\Delta T = 5$ K, with voltage polarity reversal upon magnetic-field inversion maintained throughout the range. As shown in Fig. 3a, the LSSE amplitude increases upon cooling from 300 K to approximately 150 K, whereas further cooling below 150 K leads to a pronounced reduction in the signal (Fig. 3b). Figure 3c displays the corresponding magnetic-field-dependent LSSE curves at individual temperatures, illustrating the nonmonotonic evolution of the LSSE response. Quantitatively, the LSSE voltage increases from approximately 6.7 μV at 300 K to a maximum of approximately 9.7 μV near 150 K, corresponding to an enhancement of approximately 45%. Further cooling to 25 K reduces the voltage to approximately 0.4 μV. Interestingly, a similar nonmonotonic temperature dependence was reported in our previous study of Pt/YIG and Pt/Gr/YIG heterostructures [29]. Both reference structures exhibited an enhanced LSSE response upon cooling from room temperature, followed by a decrease at lower temperatures. The present measurements extend this characteristic behavior to Pt/Gr/Gr/YIG containing two sequentially transferred Gr

monolayers. Although the absolute signal magnitudes and experimental conditions may differ, the broadly similar temperature dependence suggests that the underlying magnon-mediated contribution from YIG remains important after insertion of the additional Gr/Gr interface.

The nonmonotonic temperature dependence of V_{LSSE} may be qualitatively understood in terms of the interplay between thermally excited magnon populations and temperature-dependent magnon transport processes. At relatively high temperatures, enhanced magnon scattering and relaxation processes may limit effective magnon propagation in YIG [17, 30, 31]. Cooling toward the LSSE maximum may reduce these transport limitations, thereby favoring an enhanced spin-current response. At lower temperatures, the decreasing thermal population of magnons, together with changes in their transport properties, can contribute to the reduction of the detected LSSE signal [32, 33]. The detailed temperature profiles can be further influenced by magnon–magnon relaxation and temperature-dependent interfacial spin coupling [9, 34]. Although these mechanisms provide a plausible interpretation, the present measurements do not independently identify the dominant scattering process or determine its temperature dependence. The observation of a pronounced LSSE maximum near 150 K in Pt/Gr/Gr/YIG, together with the similar temperature-dependent behavior previously reported for Pt/YIG and Pt/Gr/YIG [29], indicates that the characteristic nonmonotonic LSSE response persists despite the additional Gr/Gr interface. When combined with the systematic suppression observed at 300 K (Fig. 2), these findings are consistent with a picture in which sequential Gr insertion modifies the overall efficiency of spin-current injection and detection without eliminating the characteristic temperature-dependent magnon-mediated response associated with YIG. However, the present results do not establish whether the effective interfacial spin transmission itself varies with temperature.

These results demonstrate that Pt/Gr/Gr/YIG retains a measurable LSSE response throughout the investigated temperature range, while exhibiting substantial suppression of its room-temperature

amplitude compared with Pt/YIG and Pt/Gr/YIG. Thus, sequential Gr insertion provides an additional interfacial parameter for controlling thermally driven spin transport in Pt/YIG-based heterostructures.

3.4. First-principles DFT calculation in Pt/Gr/Gr/NiFe structures

To examine the influence of Gr interlayers on the interfacial electronic structure, first-principles DFT calculations were performed for Pt/Gr/Gr/NiFe model heterostructures with AA- and AB-stacked bilayer Gr, as shown in Fig. 4. NiFe was employed as a simplified ferromagnetic model to introduce magnetic exchange interactions, rather than to reproduce the full electronic and magnonic properties of YIG. In our previous study [14], calculations for Pt/Gr/NiFe revealed Gr–metal hybridization and proximity-modified electronic states associated with interfacial exchange coupling and spin–orbit interactions. The present calculations extend this approach to bilayer Gr to investigate the effects of an additional Gr/Gr interface and Gr stacking on the electronic structure. Figures 4a and 4b illustrate the relaxed atomic structures of AA- and AB-stacked Pt/Gr/Gr/NiFe, respectively. Their corresponding electronic band structures are presented in Figs. 4c and 4d, with the projected contributions from Pt (blue), Gr (red), and NiFe (green) distinguished by different colors. The calculated band structures exhibit multiple electronic states near the Fermi level, with distinct band distributions for the AA and AB configurations. These differences demonstrate that the relative arrangement of the two Gr layers influences the electronic structure of the heterostructure. Compared with the previously investigated ML Gr model [14], the bilayer configurations introduce additional Gr-derived electronic states and interlayer coupling, suggesting additional electronic hybridization pathways within the Pt/Gr/Gr/NiFe structure. Thus, the calculations indicate that both Gr layer number and stacking configuration are relevant parameters for modifying the interfacial electronic environment. The experimental LSSE results provide a complementary perspective on the role of Gr interlayers in spin transport. As shown in Fig. 2, the LSSE signal is reduced to approximately 47% of

the Pt/YIG reference value after insertion of one Gr layer and to approximately 22% after insertion of two sequentially transferred Gr layers. This progressive suppression indicates that additional Gr interlayers strongly influence the overall efficiency of thermally driven spin injection and electrical detection in Pt/YIG heterostructures. Within the thermal spin pumping framework, the reduced response is consistent with a decrease in effective interfacial spin transmission, provided that the thermal driving conditions and spin-to-charge conversion efficiency remain comparable. The DFT results independently demonstrate that Gr layer arrangement modifies the interfacial electronic structure, which may influence spin-dependent interfacial coupling relevant to the observed LSSE behavior. However, the calculated band structures do not directly determine the spin mixing conductance or the LSSE voltage, and therefore cannot quantitatively explain the measured suppression ratios. Furthermore, because the experimental Gr layers were sequentially transferred, their actual stacking configurations are not established by the present calculations.

Beyond the LSSE measurements, the distinct electronic structures obtained for AA- and AB-stacked bilayer Gr (Figs 4c–d) suggest a possible route toward controlling anomalous Nernst responses. Changes in interfacial hybridization and electronic states near the Fermi level may affect the Berry-curvature distribution and the Fermi level dependence of the anomalous Hall conductivity, which are relevant to the anomalous Nernst effect (ANE). Although Berry curvature and anomalous thermoelectric transport coefficients have not been calculated here, the observed stacking dependence provides motivation for future theoretical and experimental investigations of stacking- and twist-angle-dependent ANE in Gr-based magnetic heterostructures.

4. Conclusion

In summary, we demonstrate a pronounced and systematic suppression of the LSSE through sequential insertion of Gr interlayers in Pt/YIG heterostructures. The LSSE signal decreases to

approximately 47% and 22% of its original magnitude upon insertion of one and two Gr layers, respectively, highlighting the strong sensitivity of thermally driven spin transport to atomically thin interfacial modifications. The Pt/Gr/Gr/YIG heterostructure also exhibits a nonmonotonic temperature dependence, with a maximum LSSE response near 150 K. Complementary DFT calculations of Pt/Gr/Gr/NiFe model heterostructures reveal distinct stacking-dependent changes in the electronic structure of AA- and AB-stacked bilayer Gr, providing a possible microscopic perspective on Gr-mediated interfacial electronic coupling. These findings establish sequential Gr insertion as an effective strategy for suppressing the measured LSSE response and highlight stacking engineering as a promising route toward tailoring interfacial electronic structures. Furthermore, they suggest opportunities for future investigations of stacking- and twist-angle-dependent ANE in Gr-based magnetic heterostructures.

Acknowledgements This research was supported by the Chung-Ang University Research Scholarship Grants in 2025. This study was supported by the National Research Foundation of Korea funded by the Korean Government (RS-2023-NR076951 and RS-2025-16066690).

Author Contribution S.K.L. conceived and designed the research project. J.M.C., Y.H.K., and J.W.C. fabricated the devices, performed all LSSE measurements and analyzed LSSE signals. Y.G.Y. performed first-principles DFT calculation and analyzed for Pt/Gr/Gr/NiFe heterostructure. Finally, J.M.C., Y.H.K., Y.G.Y., and S.K.L. wrote the manuscript. All authors discussed the results and commented on the manuscript.

Declaration of Competing Interest

The authors declare that they have no known competing financial interest or personal relationships that could have appeared to influence the work reported in this paper.

Data Availability

Data will be made available on request.

References

[1] K. Uchida, J. Xiao, H. Adachi, J. Ohe, S. Takahashi, J. Ieda, T. Ota, Y. Kajiwara, H. Umezawa, H. Kawai, G.E.W. Bauer, S. Maekawa, E. Saitoh, Nat. Mater., **9** (2010) 894-897.

[2] K. Uchida, S. Takahashi, K. Harii, J. Ieda, W. Koshibae, K. Ando, S. Maekawa, E. Saitoh, Nature, **455** (2008) 778-781.

[3] T. Kikkawa, K. Shen, B. Flebus, R.A. Duine, K.I. Uchida, Z. Qiu, G.E. Bauer, E. Saitoh, Phys. Rev. Lett., **117** (2016) 207203.

[4] T. Kikkawa, K. Uchida, Y. Shiomi, Z. Qiu, D. Hou, D. Tian, H. Nakayama, X.F. Jin, E. Saitoh, Phys. Rev. Lett., **110** (2013) 067207.

[5] W.-Y. Lee, N.-W. Park, M.-S. Kang, G.-S. Kim, Y.-G. Yoon, S. Lee, K.-Y. Choi, K.S. Kim, J.-H. Kim, M.-J. Seong, T. Kikkawa, E. Saitoh, S.-K. Lee, ACS Appl. Mater. Inter., **13** (2021) 45097-45104.

[6] J. Xiao, G.E.W. Bauer, K. Uchida, E. Saitoh, S. Maekawa, Phys. Rev. B, **81** (2010) 214418.

[7] T. Kikkawa, K. Uchida, S. Daimon, Y. Shiomi, H. Adachi, Z. Qiu, D. Hou, X.F. Jin, S. Maekawa, E. Saitoh, Phys. Re.v B, **88** (2013) 214403.

[8] K. Uchida, T. Kikkawa, T. Seki, T. Oyake, J. Shiomi, Z.Y. Qiu, K. Takanashi, E. Saitoh, Phys. Rev. B, **92** (2015) 094214.

[9] E.J. Guo, J. Cramer, A. Kehlberger, C.A. Ferguson, D.A. MacLaren, G. Jakob, M. Klaui, Phys. Rev. X, **6** (2016) 031012.

[10] M. Zeng, Y. Feng, G. Liang, Nano Lett., **11** (2011) 1369-1373.

[11] J.F. Sierra, I. Neumann, J. Cuppens, B. Raes, M.V. Costache, S.O. Valenzuela, Nat. Nanotechnol., **13** (2018) 107-111.

[12] Z. Wang, C. Tang, R. Sachs, Y. Barlas, J. Shi, Phys. Rev. Lett., **114** (2015) 016603.

[13] J. Park, I. Oh, L. A.-Y., H. Jang, J.-W. Yoo, Y.J. Jo, S.-Y. Park, J. Alloy Compd., **829** (2020) 154535.

[14] J.M. Cho, Y.H. Kim, K. J., D.H. Jang, J.W. Choi, G.S. Kim, S.J. Won, W.Y. Lee, N.W. Park, J.T. Nam, K.S. Kim, Y.G. Yoon, S.K. Lee, J. Alloy Compd., **1083** (2026) 191685.

[15] S.K. Lee, W.Y. Lee, T. Kikkawa, C.T. Le, M.S. Kang, G.S. Kim, A.D. Nguyen, Y.S. Kim, N.W. Park, E. Saitoh, Adv. Funct. Mater., **30** (2020) 202070239.

[16] J.W. Choi, Y.H. Kim, J.M. Cho, G.S. Kim, Y.G. Yoon, N.W. Park, K. Sugawara, J. Nam, T. Kikkawa, K.S. Kim, E. Saitoh, T. Sato, W.Y. Lee, S.K. Lee, Chem. Eng. J., **548** (2026) 181568.

[17] J.W. Choi, S.J. Won, J.M. Cho, Y.H. Kim, G. Park, D.H. Jang, N.W. Park, G.S. Kim, S. Jeon, S.K. Lee, J. Alloy Compd., 1056 (2026) 186666.

[18] B. Zhuang, S. Li, S. Li, J. Yin, Carbon, **173** (2021) 609-636.

[19] J.-H. Lee, E.K. Lee, W.-J. Joo, Y. Jang, B.-S. Kim, J.Y. Lim, S.-H. Choi, S.J. Ahn, J.R. Ahn, M.-H. Park, Science, **344** (2014) 286-289.

[20] D.Y. Lee, J. Nam, G.Y. Lee, I. Lee, A.-R. Jang, K.S. Kim, Nano Convergence, **11** (2024) 32.

[21] E. Bordes, B. Morcos, D. Bourgogne, J.-M. Andanson, P.-O. Bussière, C.C. Santini, A. Benayad, M. Costa Gomes, A.A. Pádua, Front. Chem., **7** (2019) 223.

[22] Y. Yao, Z. Li, Z. Lin, K.-S. Moon, J. Agar, C. Wong, J. Phys. Chem. C, **115** (2011) 5232-5238.

[23] A. Reina, X. Jia, J. Ho, D. Nezich, H. Son, V. Bulovic, M.S. Dresselhaus, J. Kong, Nano Lett., **9** (2009) 30-35.

[24] A.C. Ferrari, Solid State Commun., **143** (2007) 47-57.

[25] A.C. Ferrari, J.C. Meyer, V. Scardaci, C. Casiraghi, M. Lazzeri, F. Mauri, S. Piscanec, D. Jiang, K.S. Novoselov, S. Roth, A.K. Geim, Phys. Rev. Lett., **97** (2006) 187401.

[26] K.S. Novoselov, A.K. Geim, S.V. Morozov, D. Jiang, Y. Zhang, S.V. Dubonos, I.V. Grigorieva, A.A. Firsov, Science, **306** (2004) 666-669.

[27] B.B. Krichevtsov, S.V. Gastev, S.M. Suturin, V.V. Fedorov, A.M. Korovin, V.E. Bursian, A.G. Banshchikov, M.P. Volkov, M. Tabuchi, N.S. Sokolov, Sci. Tech. Adv. Mater., **18** (2017) 351-363.

[28] S. Haku, T. Tashiro, H. Nakayama, J.i. Ieda, S. Entani, S. Sakai, K. Ando, Appl. Phys. Express, **8** (2015) 073009.

[29] J.W. Choi, Y.H. Kim, J.M. Cho, K. Sugawara, J. Nam, M.S. Kang, G. Park, G.S. Kim, N.W. Park, T.

Kikkawa, W.Y. Lee, Y.G. Yoon, K.S. Kim, E. Saitoh, T. Sato, S.K. Lee, J. Mater. Chem. A, **13** (2025) 26690.
[30] H. Adachi, K.-i. Uchida, E. Saitoh, J.-i. Ohe, S. Takahashi, S. Maekawa, Appl. Phys. Lett., **97** (2010) 252506.
[31] H.J. Lee, N.R. Park, E.S. Cho, S.J. Won, K.H. Moon, Y.H. Kim, S.K. Lee, Adv. Phys. Res., e70156 (2026).
[32] H. Adachi, S. Maekawa, J. Korean Phys. Soc., **62** (2013) 1753-1758.
[33] S. Rezende, R. Rodríguez-Suárez, J. Lopez Ortiz, A. Azevedo, Phys. Rev. B, **89** (2014) 134406.
[34] S. Rezende, R. Rodríguez-Suárez, R. Cunha, A. Rodrigues, F. Machado, G. Fonseca Guerra, J. Lopez Ortiz, A. Azevedo, Phys. Rev. B, **89** (2014) 014416.

Figure captions

Fig. 1. (a) Photograph-based schematic of the sample holder and heating assembly mounted on the PPMS puck, with an enlarged cross-sectional view of the measurement configuration at position A. (b, c) Schematic illustrations of thermally generated spin-current injection and ISHE detection in Pt/YIG and Pt/Gr/Gr/YIG heterostructures, respectively. The applied temperature gradient generates a spin current ($\boldsymbol{J_s}$) from YIG toward Pt, where it is converted into a transverse electrical voltage through the ISHE. The insertion of Gr interlayers may modify interfacial spin transmission, leading to a suppressed LSSE signal. (d) High-resolution transmission electron microscopy (HR-TEM) image of as-grown ML Gr transferred onto a TEM grid. The inset shows a fast Fourier transform (FFT) pattern obtained from a well-ordered ML Gr region. (e) Raman spectra of CVD-grown ML Gr on a Cu substrate and ML Gr transferred onto a YIG/GGG substrate. Asterisks (*) indicate Raman modes originating from the YIG/GGG substrate.

Fig. 2. Magnetic-field-dependent LSSE measurements in Pt/YIG, Pt/Gr/YIG, and Pt/Gr/Gr/YIG heterostructures at 300 K. (a–c) LSSE voltage curves measured under temperature differences (ΔT) ranging from 2 to 10 K for (a) Pt/YIG, (b) Pt/Gr/YIG, and (c) Pt/Gr/Gr/YIG. (d) ΔT dependence of the LSSE voltage for the three heterostructures, showing an approximately linear relationship between V_{LSSE} and ΔT. (e) Comparison of the magnetic-field-dependent LSSE responses of the three heterostructures under identical measurement conditions. (f) Relative LSSE amplitudes normalized to the Pt/YIG reference, illustrating the successive suppression of the LSSE signal upon insertion of one and two Gr interlayers.

Fig. 3. Temperature-dependent LSSE in the Pt/Gr/Gr/YIG heterostructure measured under a nominally fixed temperature difference of ΔT = 5 K. (a) Magnetic-field-dependent LSSE voltage

curves measured between 150 and 300 K, showing an increase in the LSSE amplitude upon cooling toward 150 K. (b) Corresponding LSSE voltage curves measured between 25 and 150 K, exhibiting a pronounced reduction in the LSSE amplitude with decreasing temperature. (c) Magnetic-field-dependent LSSE voltage curves at selected temperatures from 25 to 300 K, vertically offset for clarity. The measurements reveal a nonmonotonic temperature dependence with a maximum LSSE response near 150 K.

Fig. 4. First-principles atomic and electronic structures of Pt/Gr/Gr/NiFe heterostructures with different Gr stacking configurations. (a, b) Top and side views of the relaxed atomic structures containing AA- and AB-stacked bilayer Gr, respectively. (c, d) Corresponding calculated electronic band structures for the AA- and AB-stacked configurations, respectively, presented at progressively enlarged energy scales to highlight the electronic states near the Fermi level. Blue, red, and green bands indicate Pt-, Gr-, and NiFe-dominant electronic states, respectively, based on their projected orbital contributions. The dashed vertical lines indicate the high-symmetry point in the Brillouin zone. The calculations illustrate stacking-dependent modifications of the interfacial electronic structure.

Figure 1

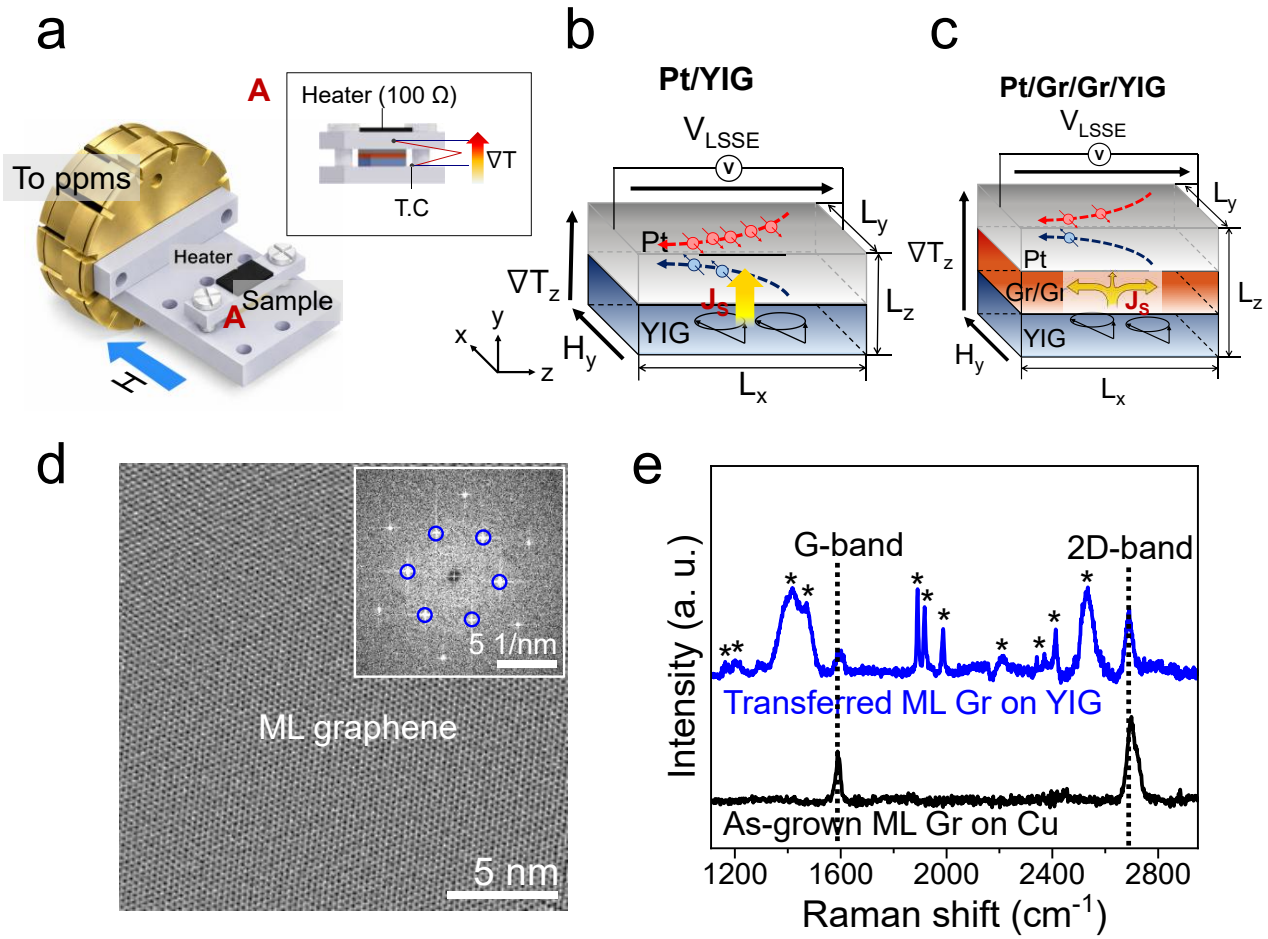

a
b
c
A
Heater (100 Ω)
∇T
T.C
To ppms
Heater
Sample
A
H
Pt/YIG
V_{LSSE}
V
L_y
Pt
J_s
∇T_z
L_z
YIG
x
y
z
H_y
L_x
Pt/Gr/Gr/YIG
V_{LSSE}
V
L_y
∇T_z
Pt
Gr/Gr
J_s
L_z
YIG
H_y
L_x
d
5 1/nm
ML graphene
5 nm
e
G-band
2D-band
Intensity (a. u.)
Transferred ML Gr on YIG
As-grown ML Gr on Cu
1200
1600
2000
2400
2800
Raman shift (cm^{-1})

Figure 2

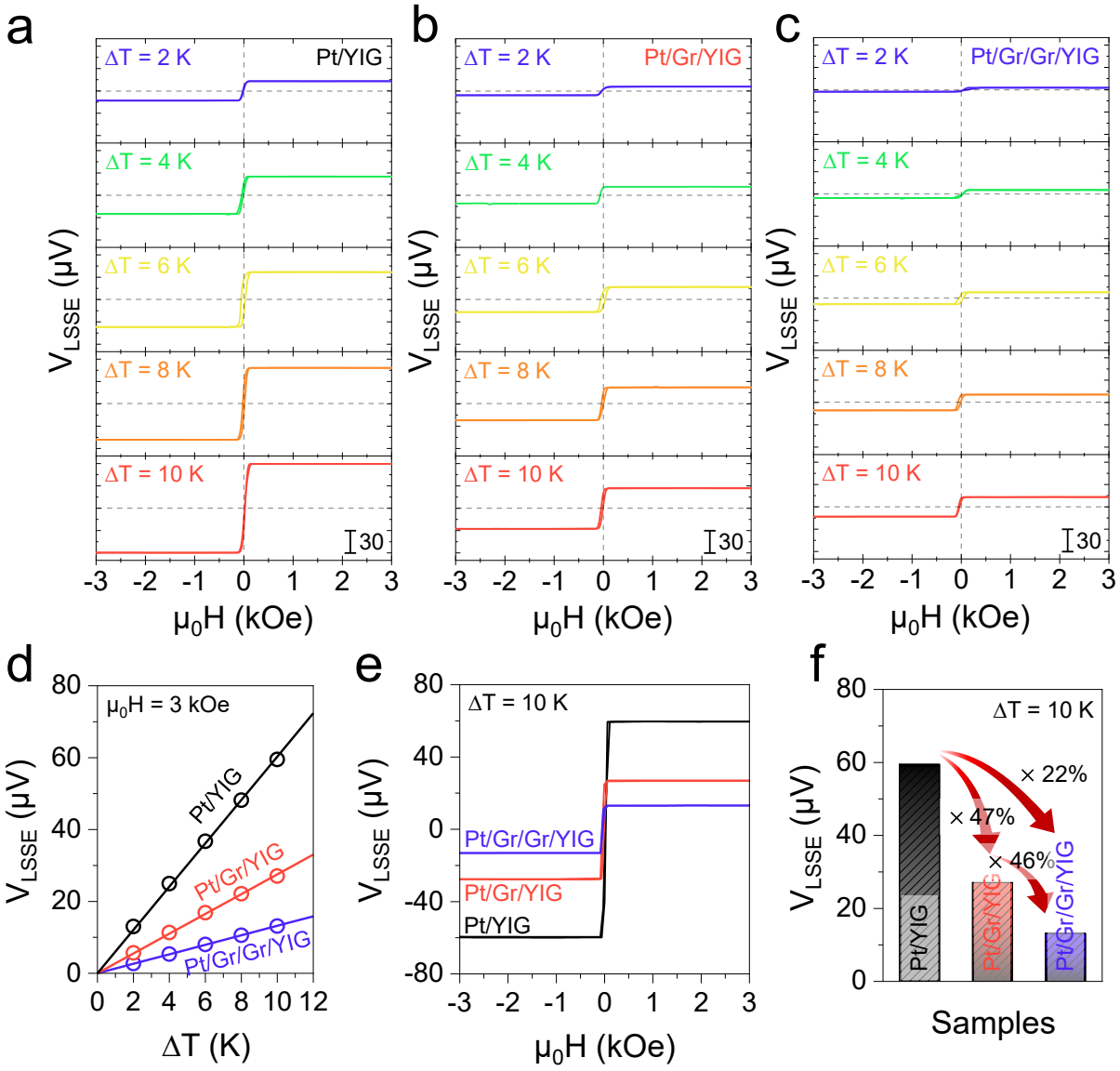

a
b
c
ΔT = 2 K
ΔT = 4 K
ΔT = 6 K
ΔT = 8 K
ΔT = 10 K
Pt/YIG
Pt/Gr/YIG
Pt/Gr/Gr/YIG
30
V_LSSE (μV)
μ0H (kOe)
d
e
f
μ0H = 3 kOe
ΔT (K)
ΔT = 10 K
Pt/YIG
Pt/Gr/YIG
Pt/Gr/Gr/YIG
× 47%
× 22%
× 46%
Samples

Figure 3

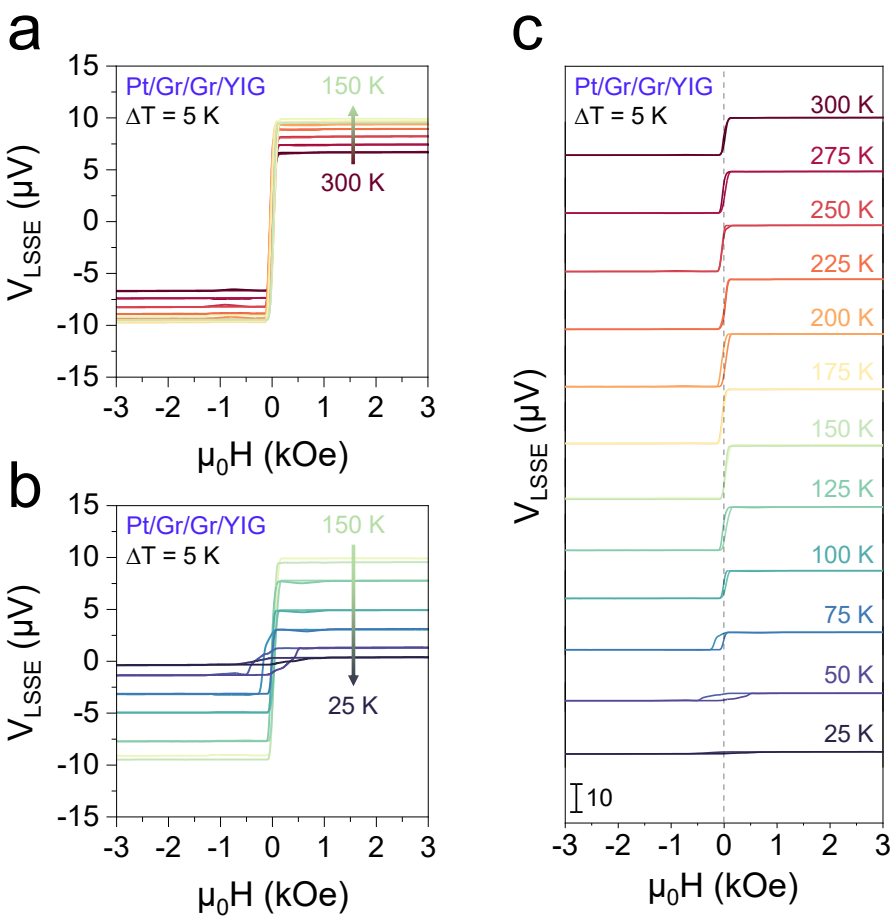
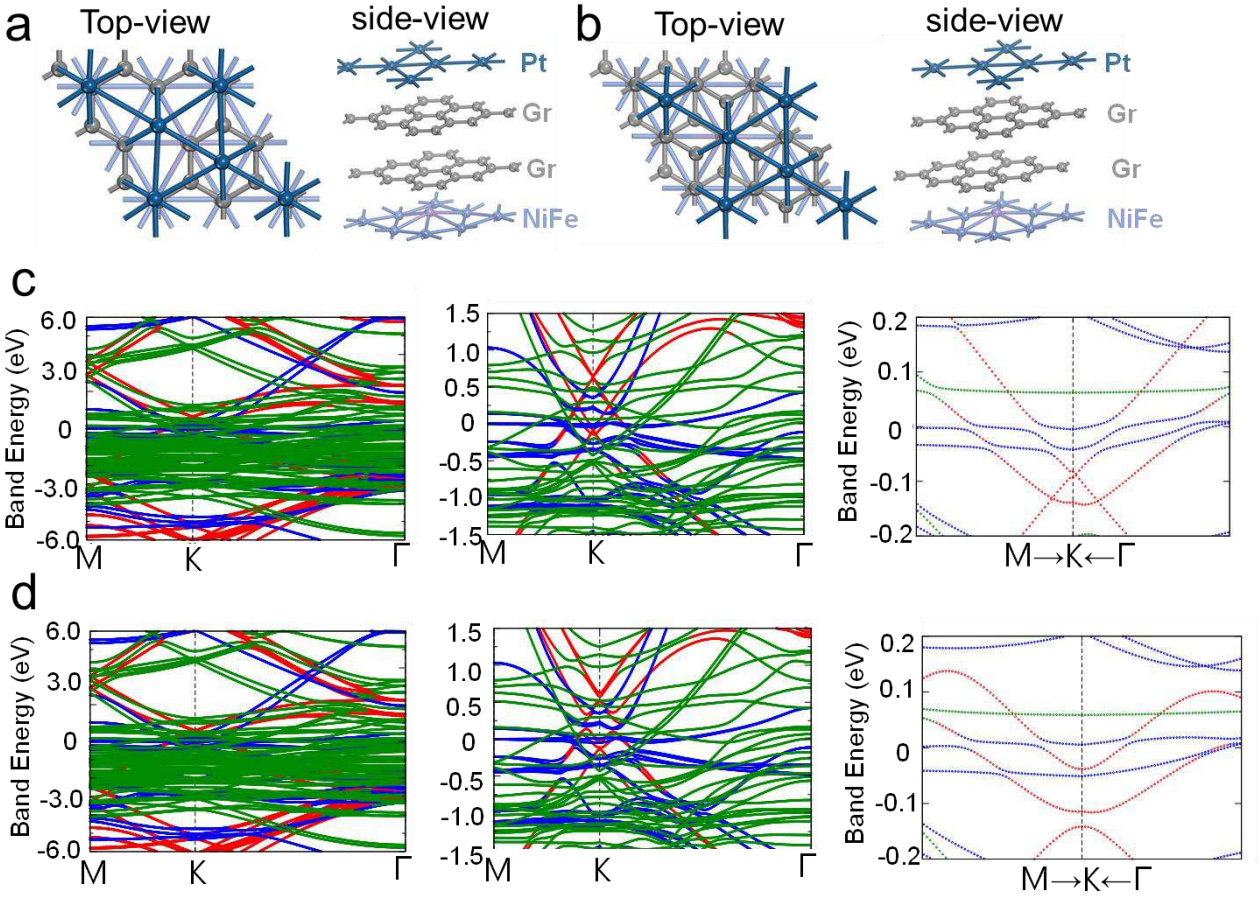

a
b
c
Pt/Gr/Gr/YIG
ΔT = 5 K
150 K
300 K
25 K
V_{LSSE} (μV)
$μ_0H$ (kOe)
275 K
250 K
225 K
200 K
175 K
125 K
100 K
75 K
50 K
10

Figure 4


a
Top-view
side-view
Pt
Gr
Gr
NiFe
b
Top-view
side-view
Pt
Gr
Gr
NiFe
c
Band Energy (eV)
6.0
3.0
0
-3.0
-6.0
M
K
Γ
1.5
1.0
0.5
0
-0.5
-1.0
-1.5
M
K
Γ
Band Energy (eV)
0.2
0.1
0
-0.1
-0.2
M→K←Γ
d
Band Energy (eV)
6.0
3.0
0
-3.0
-6.0
M
K
Γ
1.5
1.0
0.5
0
-0.5
-1.0
-1.5
M
K
Γ
Band Energy (eV)
0.2
0.1
0
-0.1
-0.2
M→K←Γ